Biosensors and Bioelectronics 142 (2019) 111494

Contents lists available at ScienceDirect

Biosensors and Bioelectronics

journal homepage: www.elsevier.com/locate/bios

Protein binding kinetics quantification via coupled plasmonic-photonic resonance nanosensors in generic microplate reader

Tang Dang[a,1], Wenjun Hu[a,1], Wei Zhang[a], Zifang Song[b], Yi Wang[c], Mingqian Chen[a], Hao Xu[c,**], Gang Logan Liu[a,*]

[a] School of Life Science and Technology, Huazhong University of Science and Technology Wuhan, Hubei, 430074, China
[b] Department of Hepatobiliary Surgery, Union Hospital, Tongji Medical College, Huazhong University of Science and Technology, Wuhan, China
[c] Liangzhun (Shanghai) Industrial Co. Ltd, Shanghai, China

ARTICLE INFO

Keywords:
Protein binding kinetics
Surface plasmon resonance
Nanophotonics
C-reactive protein
Sandwich immunoassay

ABSTRACT

Almost no analytical assays, either colorimetric or fluorescence assays, for generic microplate readers is capable of dynamic measurements of protein-protein binding or the quantification of kinetic association and dissociation constants of protein interactions. On the other hand, protein binding kinetics quantification can be uniquely done on special expensive surface plasmon resonance (SPR) sensing equipment. Here we report the integration of coupled plasmonic-photonic resonance nanosensors in standard 96-well plate format and by using which, for the very first time, the demonstration of label-free dynamic SPR-like protein binding measurement and kinetics quantification in a generic microplate reader. Our low-cost label-free nanosensor plate enables very sensitive detection of immobilized protein interactions based on the transmission optical density (OD) value changes at specific wavelengths measured in a generic microplate reader. The relative end-point OD value changes show a good linear response with protein concentrations (from 0.05 to 50 μg/ml). And the protein quantification in serum results are consistent with the concurrent hospital lab tests. Most importantly, the kinetic association and dissociation constants of protein interactions in our sensor plate wells are determined by time-lapse dynamic OD value measurement in the generic microplate reader. Enabled by our unique nanosensor plate, SPR-like measurement of protein binding kinetics is now available using generic microplate reader ubiquitous in many chemistry and biomedical research labs.

1. Introduction

Measurements of molecular interactions kinetics is increasingly important in drug discovery (Arlett et al., 2011), genetic screening (D'Orazio, 2003) and clinical diagnostics (Cheng et al., 2006) because the dynamic binding information improves understanding of diseases and can provide new ideas for treatment (Boccaletti et al., 2006). Surface plasmon resonance (SPR) sensors such as the commercial Biacore SPR biosensor system are capable of real-time monitoring kinetic biomolecular interactions, requiring no labeling and unaffected by bulk background while collecting high quality time-lapse data of surface biomolecular and drug binding events (Jason-Moller et al., 2006; Leonard et al., 2011). Conventional SPR sensors are typically gold or silver thin films deposited on glass or other dielectric substrate (Homola, 2008). Notably as a result of the surface molecular binding event, small plasmon resonance angle or resonance wavelength shifts due to a change in refractive index near the SPR sensor chip surface. Many SPR research papers reported the protein sensitivity is ng/ml or even low (Wang et al., 2017). Although high-precision optics and optomechanical components in conventional SPR instrumentation such as Biacore and Bio-rad ProteOn system allow the detection of the real-time small resonance angle or wavelength shift on gold thin film sensor during surface protein interactions, the reliable sensitivity is still limited to μg/ml concentration level. The modest molecular sensitivity and exceptional instrument requirement prevent wider analytical applications of conventional SPR sensing in both applied and fundamental biomedical research as well as clinical diagnostics.

On the other hand, metallic periodic nanostructures and nanoparticles can also be used as plasmonic biosensor (Maynard et al., 2009), known as localized surface plasmon resonance (LSPR) sensors.

* Corresponding author.
** Corresponding author.
E-mail address: loganliu@hust.edu.cn (G.L. Liu).
[1] These authors contributed equally.

https://doi.org/10.1016/j.bios.2019.111494
Received 13 May 2019; Received in revised form 21 June 2019; Accepted 4 July 2019
Available online 05 July 2019
0956-5663/

LSPR is an optical phenomenon caused by collective oscillation of electron gas in a metal nanostructure surrounded by dielectric material (Bohren and Huffman, 1983). Compared to conventional SPR, LSPR doesn't need a prism or other optical coupling device to excite and has higher surface-to-volume ratio (Yeom et al., 2013). These features of LSPR sensors make it possible for detections in ubiquitous laboratory equipment.

Measuring the binding kinetics and quantification of various protein biomarkers in biofluids is essential for effective diagnostics, targeted therapeutics and prognostics besides of drug development and screening. For example, C-reactive protein (CRP) is a calcium-dependent pentameric ring-shaped molecule, which consist of five identical non-glycosylated polypeptide sub-units (Pepys and Hirschfield, 2003). It is known as a biomarker for many diseases of cardiovascular (Ridker et al., 1998), respiratory (Crystal et al., 1984), metabolic disorders (Hotamisligil, 2006) and has been proved useful in the effectiveness of the treatments. The cutoff value of CRP level in blood for a healthy person is 5 μg/ml (Meyer et al., 2006). During the acute-phase response of inflammation, the CRP concentration in blood abruptly increases to 600–1000 μg/ml and reaches the peak after about 48 h (Reeves, 2007).

In this paper, we demonstrate a label-free LSPR biosensor in the 96-well plate format for dynamic measurements of CRP and anti-CRP antibody binding kinetics only using a ubiquitous generic microplate reader, and at the same time quantification of CRP concentration in buffer and blood serum is performed. We simply used antibody-target protein-antibody sandwich method in the 96-well LSPR sensor plate as shown in Fig. 1a–c and measure the dynamic change of OD value by a generic microplate reader to carry out similar kinetic protein measurements in conventional SPR systems such as Biacore. Fig. 1d shows that different media will present different colors on the sensor chip. After our nanoplasmonic 96-well plate device is manufactured, CRP capture antibodies were immobilized on the microwell bottom surface. The secondary antibody is used for dynamic measurement and improving the sensitivity and specificity. The protein binding kinetics measurement on the 96-well plate sensor reaches a limit of detection (LOD) of 50 ng/ml, at least 2 orders of magnitude below the CRP levels in plasma and also below the LOD of Biacore systems. Our study paves the way for the high-throughput, low-cost and ubiquitous SPR protein characterization, binding interaction and dynamic analysis in microplate readers.

2. Experimental

2.1. Reagents

Hexylsilane, streptavidin, isopropanol, ethanol, sucrose, 6-mercapto-1-hexanol (MCH), 11-mercaptuoudecanoic acid (MUA), 1-ethyl-3-(dimethylaminopropyl)carbodiimide (EDC), N-hydroxysuccinimide (NHS), bovine serum albumin (BSA), ethanolamine, purified CRP and phosphate-buffered saline (PBS) buffer were purchased from Sigma-Aldrich, thiolated biotin was purchased from Nanocs, monoclonal anti-CRP capture and detection antibody was purchased from Sino Biological. All chemicals were used as received without any further purification. The patient blood samples were obtained from Wuhan Union Hospital.

2.2. Fabrication process

The nanoplasmonic sensor film is fabricated by a replica molding process and parameters of sensor chip are described in Supporting Information. The original mold was a tapered nanopillar array on silicon oxide wafer by laser interference lithography and ion etching. Prior to replication, the mold was put into a vacuum dryer full of hexylsilane 12 h for hydrophobicity. Then, spread the Norland optical adhesive (NOA-61) evenly on the mold and place a polyethylene terephthalate (PET) sheet on the top of it. After 3 min of UV light (105 mW/cm^2) irradiation, peel off the PET sheet. Then, multiple layers metal and oxide were deposited onto the nanocup array. Cut the chip into small pieces of 1 cm × 1 cm, stick the chip to an open-bottom 96-well plate which was made by a 3D printer (Object 30 primer™ Stratasys Ltd.) to form unique nanosensor plate.

2.3. Biotin-streptavidin binding

Prior to the experiment, rinse the chip integrated microplate wells twice with isopropanol and deionized (DI) water. Incubated the chips in a 1 mM thiolated biotin (in PBS) for 3 h at room temperature followed by immersion in 1 mM MCH (in DDW) blocking solution for 1 h at room

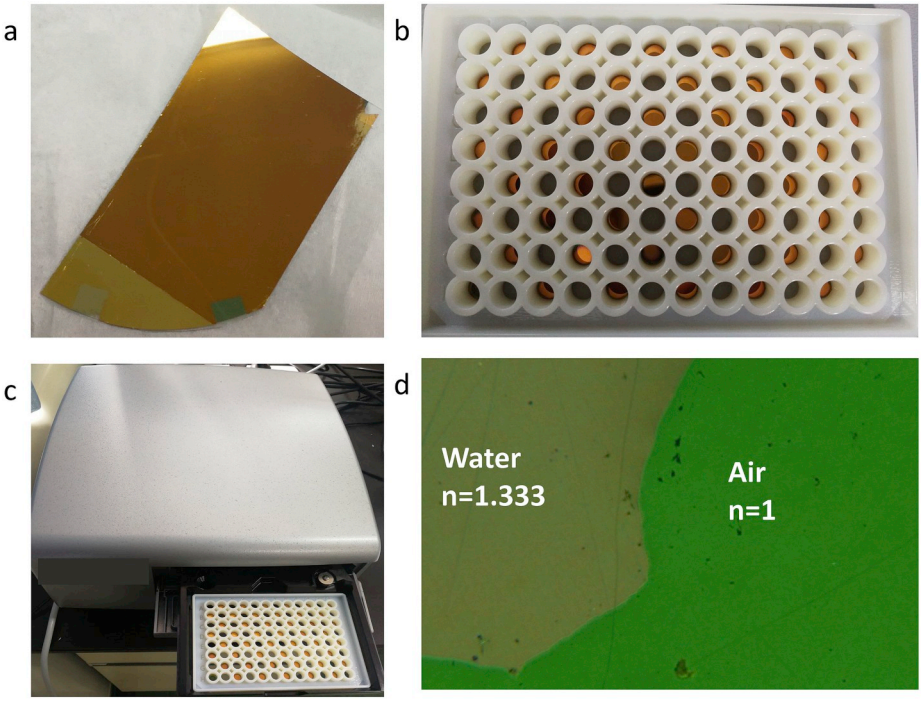

Fig. 1. Overview of the Au-TiO_2 -Au nanocup array chip and protocol. (a) Photograph of one piece of Au-TiO_2 -Au nanocup array chip. (b) Integrate the Au-TiO_2 -Au nanocup array chip with a homemade 96-well plate. (c) Test with a simple small volume microplate reader. (d) Transmission microscopy image. Air and water on the device surface show different colors, green and olive, respectively. (For interpretation of the references to color in this figure legend, the reader is referred to the Web version of this article.)

temperature. Finally, the chips were immersed respectively in a 5 μg/ml and 50 μg/ml streptavidin solution (in PBS) at room temperature for 30 min and the binding kinetics of streptavidin was measured with respect to time by dynamic curve function (one point every 10s) of the microplate reader. The chips were washed twice with DI water and after washing, an end-point absorption spectrum was measured using phosphate buffered solution in micro plate wells following each step.

2.4. CRP-antibody binding kinetics and quantification

Prior to the experiment, rinse the chip twice with isopropanol and deionized (DI) water. Incubate the chips in a 1 mM MUA solution (in ethanol) for 12 h at room temperature. Clean the chips with 70% ethanol and DI water twice, and afterwards measure the absorption spectrum in DI water. Incubate the chips in a mixture of 400 mM EDC and 100 mM NHS for 30 min at room temperature and then incubate 60 μg/ml monoclonal anti-CRP capture antibody (in PBS) for 12 h at 4 °C. Rinse the chips with PBS and DI water, and afterwards measure the absorption spectrum in DI water. Incubate the chips in 60 μg/ml BSA blocking solution and then in 10% ethanolamine solution, and both steps last for 30 min at room temperature. Rinse the chips with DI water twice, and afterwards measure the absorption spectrum in DI water. Incubate the chips in different concentrations of CRP (in PBS) for 3 h and measure the dynamic absorption spectrum with respect to time. Rinse the chips with PBS and DI water, afterwards, measure the absorption spectrum in DI water. Finally, incubate the chips in 60 μg/ml monoclonal anti-CRP detection antibody (in PBS) and measure the absorption spectrum with respect to time. Rinse the chips with PBS and DI water, afterwards, measure the absorption spectrum in DI water. Detection of CRP in human serum samples is similar to the protocol described previously, but for the CRP capturing step, we add the human serum samples diluted 10 times with PBS instead of standard solution in PBS. IRB Ethical approval was granted by the Huazhong University of Science and Technology (Certificate #: S1029). Plasma samples were obtained by centrifuging the blood samples at 2500 × *g* and 4 °C for 15 min. The serum samples were stored at -80 °C.

3. Results and discussion

3.1. Fabrication of the Au-TiO2 -Au nanocup array chip sensor

The sensor is fabricated by combining a metal-insulator-metal multi-layer and a 3D nanocup array structures. Fig. S1a shows the schematic of the chip fabrication, spread the UV-curable polymer evenly on the mold and place a PET sheet on the top of it. After UV light irradiation and polymer solidification, peel off the PET. Then, we deposit 90 nm gold (Au), 80 nm TiO_2 and 90 nm Au on it. Au is chosen due to the visible plasmon resonance and reliable surface functionalization (-SH) while TiO_2 has high RI, low extinction coefficient and good manufacturability. Fig. S1b shows atomic force microscope (AFM) images of the sensor, and Figs. S1c–e show scanning electron microscope (SEM) images of the sensor from the top and cross-sectional view. From the AFM and SEM images, we can see a high uniformity cup array structure and each nanocup has the similar morphology. Three metal layers on the top of nanocup and nanoparticle in the cup structure can be seen in Fig. S1e.

3.2. Optical characterization

In order to know the optical response of the chip in microplate wells, 0%–60% sucrose solutions, which corresponds to the RI from 1.33 to 1.44, were prepared. Fig. 2a shows the absorption spectrum of different concentrations of sucrose solutions measured by a generic microplate reader. With the RI increase, we can see the transmission intensity increase around 560 nm, meanwhile, the intensity decrease can be observed around the wavelength about 705 nm. Fig. 2b shows the good linearity between the OD values at the resonance wavelength and RI of liquid. The sensitivity can be calculated by the relative change in the transmission intensity (T) per RI unit (RIU), and the relative transmission intensity can be calculated by 10^{-OD}. The calculated sensitivity of the sensor is 566 Δ%T/RIU at λ = 565 nm while 450 Δ%T/RIU at λ = 705 nm. The intensity changes in 565 nm and 705 nm trend inversely, so in the latter experiment, the change of OD value at 705 nm and that value at 565 nm is subtracted from each other to further improve sensitive and reduce the error caused by ambient light source intensity fluctuation and temperature variation.

We also use a three dimensional finite-difference time-domain (3D-FDTD) software to simulate the transmission spectrum and electric field distribution for sensor chip with different environment RI, specific details about simulation can be found in supporting information. Fig. 2c shows the simulated transmission spectrum with increasing RI of the superstrate. The transmission intensity decreases around 600 nm peak whereas increases around 700 nm peak, which agrees well with the experimental results. Cross-sections of the near-field electric field distributions at peak (i) and peak (ii) are shown in Figs. S2 and S3. The magnitudes of the electric field show the trends consistent to transmission light intensity.

3.3. Detection of biotin-streptavidin interaction

We tested our device in studying biotin-streptavidin interaction which has been studied a lot before and known for high affinity to demonstrate the capability for detecting kinetic biomolecular interaction as shown in Fig. 3a. We immersed the chip-in-microwell sensor with thiolated biotin to form a uniform self-assembled monolayer (SAM). Then, MCH was added to block nonspecific binding. Finally, the sensor microwell were loaded with 5 μg/ml and 50 μg/ml streptavidin respectively and a plate reader measured the OD value of 565 nm and 705 nm every 10 s. The absorption spectrum of 50 μg/ml streptavidin loading is shown in Fig. 3b. The OD@565 nm - OD@705 nm values at each step of 50 μg/ml biotin-streptavidin binding experiment are shown in the bar graph in Fig. 3c. From Fig. 3b and c, we can see there were increase of OD value due to surface binding of biotin and slight decrease following MCH surface passivation step. The biotin-streptavidin interaction is detected by an increase of 565 OD-705 OD values when adding streptavidin. Fig. 3d showed the OD-converted relative transmission intensity change at resonant wavelength with respect to time.

3.4. Detection of C-reactive protein (CRP) in buffer

Common techniques used for CRP measurement in clinics are immunonephelometry and immunoturbidimetry (Koivunen and Krogsrud, 2006). Other techniques, such as field effect transistors (Justino et al., 2013), chemiluminescence (Ala-Kleme et al., 2006), electrochemical impedance spectroscopy (Songjaroen et al., 2016), ELISA (Williams Jr and Muddiman, 2009), fluorescence (Christodoulides et al., 2005), quartz crystal microbalances (Ding et al., 2013), magnetic particles (Phurimsak et al., 2014) and SPR(Choi et al., 2015) have been also described in literature. Previous techniques have successfully detected CRP but present different shortcomings. But SPR sensors do not require the labeling process and are unaffected by electromagnetic interference, in addition, they are useful for the real-time monitoring interactions between biomolecular and studying interaction kinetics.

The CRP blood level varies from 0 to 5 μg/ml in healthy person (Food et al. 2016). In order to make a reliable detection of CRP, LOD at least an order of magnitude lower than the border value is required. A schematic of the CPR detection protocol is shown in Fig. 4a. First, the sensor chip was immersed with 1 mM MUA solution to form a SAM. EDC and NHS were added to activate carboxyl group, and then anti-CRP capture antibody was covalently bound to the surface. The chip was then incubated in BSA blocking solution and ethanolamine to block nonspecific binding and cap remaining NHS, respectively. Then, a series

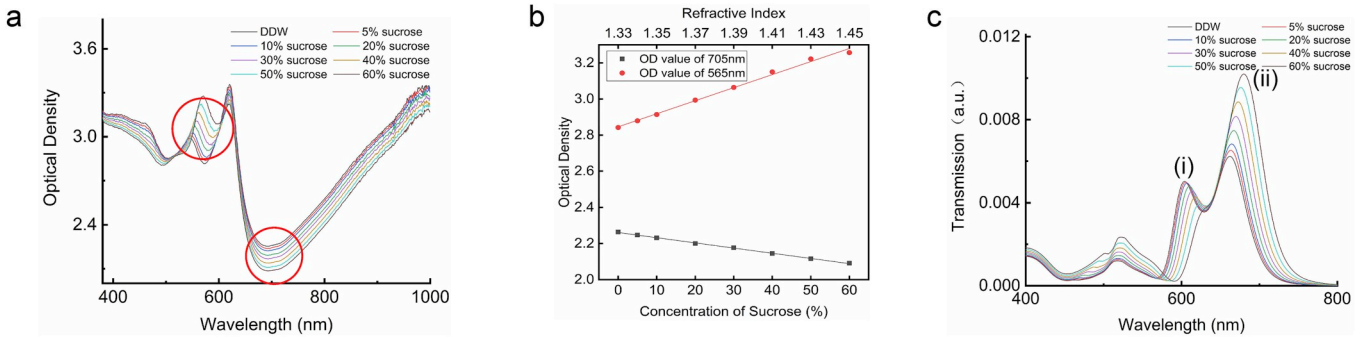

Fig. 2. (a) Measured absorption spectra of sensor chip in microplate wells with different concentrations of sucrose (0,5%,10%,20%,30%,40%,50%,60%). (b) The OD change of the Au-TiO_2 -Au nanocup array chip at 565 nm and 705 nm with respect to the different concentrations of sucrose and RI. (c) Simulation transmission spectra of sensor chip with different concentrations of sucrose.

of concentrations of CRP solutions from 0.05 μg/ml to 50 μg/ml were incubated on the sensor chip in microplate wells and the generic plate reader measured the OD value of resonant wavelength every 3 min. Finally, anti-CPR detection antibody was incubated on the sensor chip and the OD value at resonant wavelength is measured every 3 min. The spectra for PBS, 0.5 μg/ml CRP and 25 μg/ml CRP cases are presented in Fig. S4.

For the CPR capturing step, we were able to distinguish between different concentrations of CPR from 1 μg/ml to 50 μg/ml as shown in Fig. 4b. The LOD of this step is 1 μg/ml. Fig. 4c showed a plot of the relative OD value change as a function of CRP concentration on a log scale. The results were fit to a linear and showed good agreement from 1 μg/ml to 50 μg/ml. Fig. 4d showed a plot of the relative transmission intensity change values as a function of time after the CRP loading and 50 μg/ml CRP resulted in approximately 4% relative transmission intensity change. Only 4% relative transmission intensity changed and the LOD was only 1 μg/ml for the CRP detection, which is not reliable enough to confirm whether a person is healthy or not. As a consequence, we had to find a new way to extend the capability of the sensor chip. Here, we introduced another anti-CRP antibody to the sensor chip in microplate wells to form antibody-antigen-antibody sandwich structure. Due to simultaneous binding of two antibodies, the sensors have extremely high specificity and render it suitable for direct detection in complex blood serum.

A more obvious change of OD and lower LOD can be observed as shown in the bar graph Fig. 4e. The relative OD value change of 10 μg/ml CPR is only 0.02 for the CRP capturing whereas 0.103 for the anti-CRP detection antibody adding. The relative OD value change and sensitivity has increased more than 4 times. The reason of this phenomenon may be caused by more reaction sites or larger conformation changes. A plot of the relative OD value change as a function of CRP concentration on a log scale was shown in Fig. 4f. The coefficient of determination (R^2) for fitting was found to be 0.980 from 0.05 μg/ml to 25 μg/ml. The calibration equation can be expressed as $c(CRP) = 10^{-1.26148+\frac{relative\ \ OD\ \ change}{0.04268}}$.The relative OD value change of 50 μg/ml CRP was slightly higher than 25 μg/ml CRP, which indicated that the saturation was reached when adding 50 μg/ml CRP. Fig. 4g shows relative transmission intensity change over time for anti-CRP detection antibody adding. Similarly, we can see the curve of 25 μg/ml and 50 μg/ml CRP overlapping, which is corresponding to the result in Fig. 4e and f. Table S1 summaries some of the most detailed results of CRP detection reported in literature. As we know, the methods with low LOD of CRP often need labels or complex costly equipment. Our device is able to detect 50 ng/ml CRP without any label or complicated equipment which makes it convenient for research and clinical labs.

3.5. Kinetics quantification of C-reactive protein (CRP)

The SPR technology is widely used in the pharmacokinetic drug profiling (Fabini et al., 2016) and high-throughput screening (Nguyen et al., 2015). Because the SPR system can give information of the rate of interaction and the binding level, the kinetic constants can be determined (Wijaya et al., 2011). It can greatly help the rational design of new molecules of therapeutic interest and distinguish the therapeutic differentiation between similar drug compounds (Olaru et al., 2015). Similarly, our unique nanosensor microwell plate can be applied in pharmaceutical and kinetic analysis. The kinetic constants can be

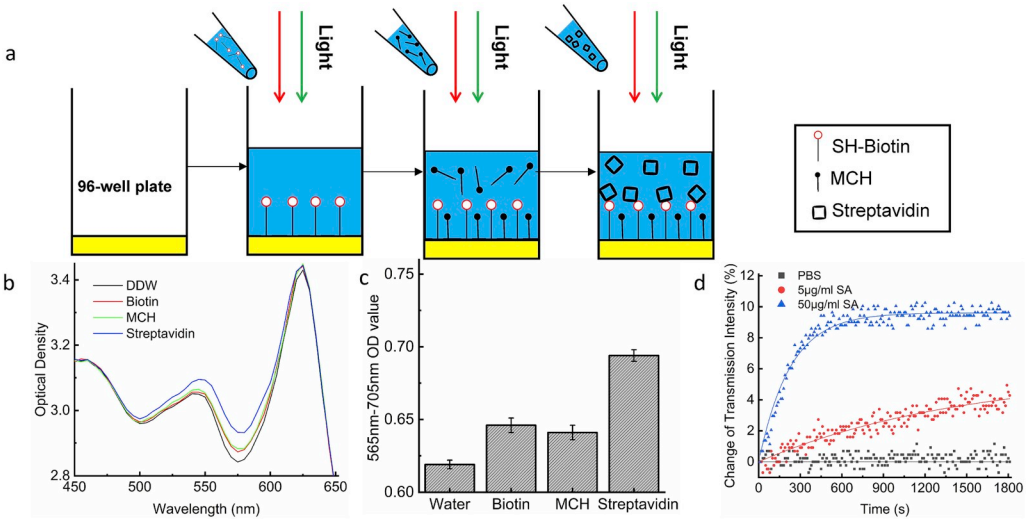

Fig. 3. (a) Schematic of Au-TiO2-Au nanocup array chip in microwell plate for biotin-streptavidin binding detection. (b) Spectra around 565 nm at different steps in 50 μg/ml streptavidin loading. (c) Bar graph of the OD value of 705 nm subtracted from the OD value of 565 nm with different step (d) Dynamic transmission intensity change at resonant wavelength with different concentrations of streptavidin binding with respect to time.

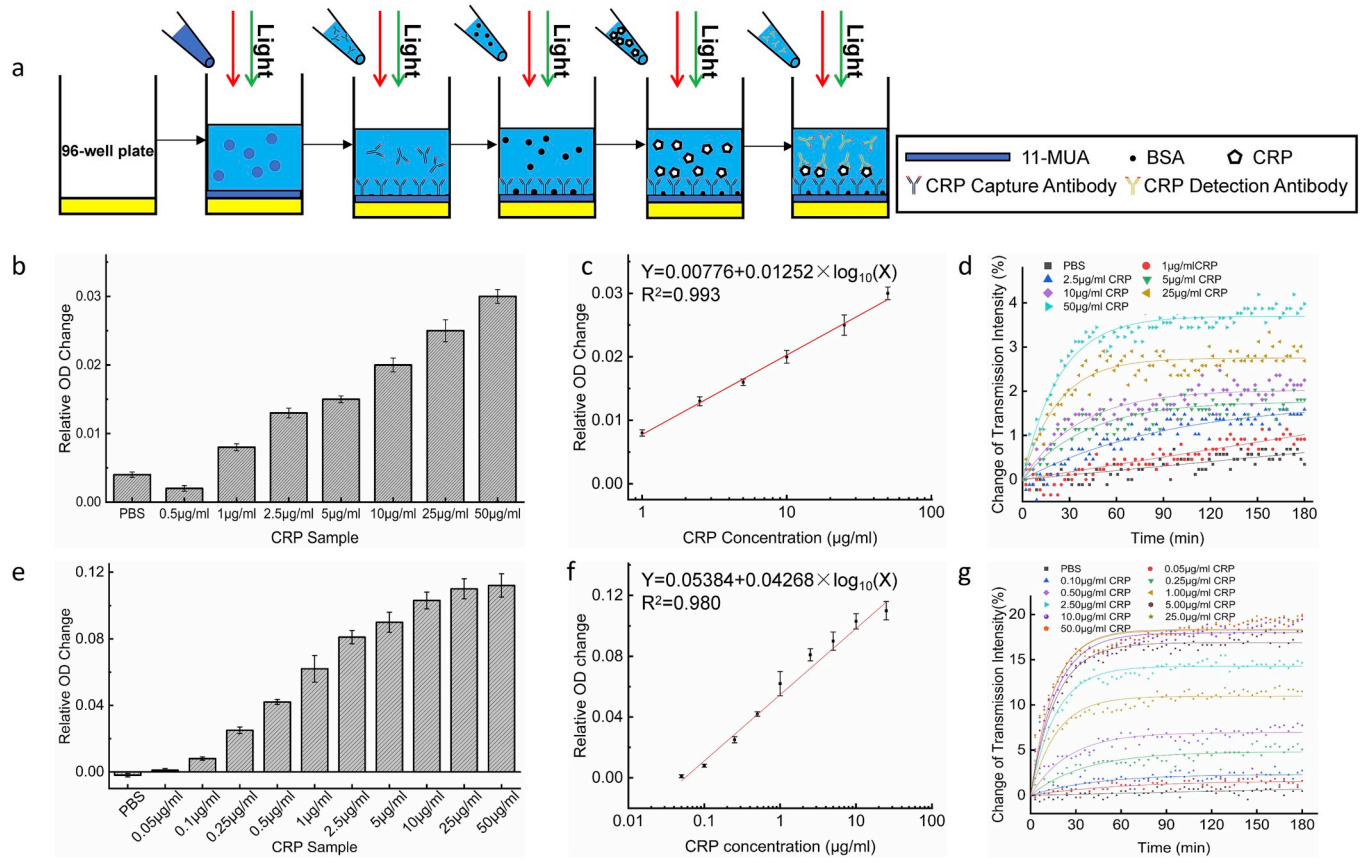

Fig. 4. Detection of CPR with noplasmonic sensor chip by microplate reader. (a) Schematic of CRP detection using two different antibodies. (b) and (e) Bar graph showing the relative OD value change for CRP sample with different concentrations and the vehicle control (PBS) at CRP immobilization step (b) and detection step (e). (c) and (f) Plot of the relative OD value change as a function of CRP concentration on a log scale. The linear curve shows the least squares fit with R^2 = 0.993 and 0.980 at CRP immobilization step (c) and detection step (f), respectively. (d) and (g) Plot of the percentage of transmission intensity change at the resonant wavelength for CRP sample with different concentrations at CRP immobilization step (c) and detection step (f).

determined from Fig. 4g. The biomolecular interactions between CRP and the detection antibody (DA) can be modeled with the following equation:

$$d[DA - CRP]/dt = k_a[DA][CRP] - k_d[DA - CRP] \quad [1]$$

Where k_a is the association rate constant, k_d is the dissociation rate constant. And the relative transmission intensity change (R) is proportional to formation of [DA-CRP]. Equation [1] can be rewritten as (O'Shannessy et al., 1993):

$$R_t = \frac{[CRP]k_a R_{max}\left[1 - e^{-([CRP]k_a + k_d)t}\right]}{[CRP]k_a + k_d} \quad [2]$$

R_{max} can be inferred by the relative transmission intensity change for 50 μg/ml CRP situation due to the sensor chip reached saturation. And plots were fitted in Fig. 4g with exponential functions y = a (1-e^{-bx}), the specific information about the fitting can be found in Table S2. If the concentration of CRP is close to saturation which corresponds to the fitting coefficient a is larger than 90% of R_{max} and the coefficient of determination (R^2) for fitting is lower than 0.65, the calculated values of k_a and k_d would has lower accuracy. In our case, 0.05 μg/ml CRP (R^2 = 0.587) shows poor fitting, 5 μg/ml (a = 92.0% R_{max}) and 10 μg/ml (a = 97.9% R_{max}) CRP are close to saturation, so when we calculated the average k_a and k_d, the data of 0.05 μg/ml, 5 μg/ml and 10 μg/ml has been discarded. Therefore, the value of k_a and k_d were calculated as 3.11×10^6 ($\pm$ 0.40×10^6) $M^{-1}s^{-1}$ and 2.00×10^{-2} ($\pm$ 0.26×10^{-2}) s^{-1}, respectively, and specific results were presented in Table 1. The dissociation equilibrium constant K_D is determined using the formula: $K_{D2} = k_a/k_d = 6.44 \times 10^{-9}$ ($\pm$ 0.38×10^{-9})M, which is an order of magnitude lower than the K_{D1} value ($6.42 \times 10^{-8} \pm 1.06 \times 10^{-8}$) of the CRP capture antibody- CRP reaction. The specific information about the kinetic constants of the CRP capture antibody- CPR reaction can be found in Table S3. The K_{D2} value is similar to the value measured by thermophoretic immunoassay (Lee et al., 2018), nanoparticle amplified SPR imaging aptasensor (Vance and Sandros, 2014), electrochemical impedimetric biosensor (Bryan et al., 2013) and fiber optic biosensor (Chou et al., 2007).

Table 1
Values of k_a, k_d and K_{D2} determined for the interaction of anti-CRP detection antibody and CRP.

[CRP](μg/ml)	k_a (10^6 $M^{-1}S^{-1}$)	k_d (10^{-2} s^{-1})	K_{D2} (10^{-9} M)
0.05	3.23 ± 0.21	1.47 ± 0.19	4.55 ± 0.51
0.1	3.39 ± 0.35	2.07 ± 0.21	6.11 ± 0.12
0.25	3.38 ± 0.15	2.10 ± 0.35	6.20 ± 1.00
0.5	3.40 ± 0.36	2.48 ± 0.25	7.29 ± 0.24
1	3.29 ± 0.21	1.99 ± 0.32	6.05 ± 0.89
2.5	2.11 ± 0.12	1.38 ± 0.14	6.54 ± 0.55
5	1.25 ± 0.13	0.55 ± 0.12	4.40 ± 0.84
10	0.67 ± 0.03	0.21 ± 0.03	3.13 ± 0.43
Average	3.11 ± 0.40	2.00 ± 0.26	6.43 ± 0.38

3.6. Blood serum sample accuracy test

To evaluate the accuracy of the chip sensor for CRP detection, some blood serum samples from healthy volunteers and sick patients were collected. They were taken blood and the concentrations of CRP is

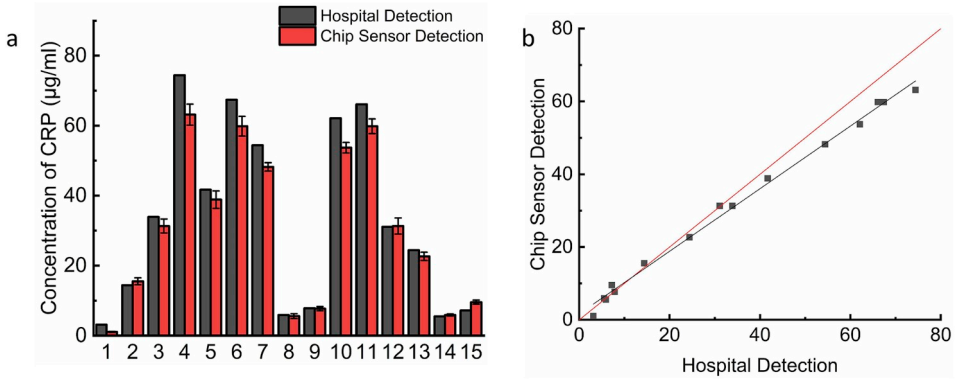

Fig. 5. Detection of CPR in blood serum with nanoplasmonic sensor chip in microplate well. (a) Measurement of CPR with different blood serum samples by sensor chip in lab and latex agglutination in hospital. (b) Comparison between lab detection and hospital detection.

quantified by latex agglutination in Wuhan Union Hospital. A portion of the blood will be used for detecting CRP by our nanoplasmonic sensor chip in microwell plate. First, the blood samples were centrifuged at 2500 × *g* and 4 °C for 15 min. Supernatant was diluted 10 times with PBS. 15 blood samples were quantified in our lab and in the hospital, respectively, and the comparative results are shown as Fig. 5a. We can see our sensor chip showed more consistency with hospital test results at low concentrations of CPR, but at high concentrations of CPR, the values detected from our sensor were lower than those from hospital test. It may be explained by strong non-specific surface adsorption competing with CRP in blood serum. Fig. 5b showed the good correlation (R^2 = 0.994, y = 0.86x + 1.636) between the results from the sensor chip and reports from hospital. Furthermore, the LOD of the hospital report was 3.1 μg/ml (sample 1), the value less than 3.1 μg/ml was considered within the normal range. But our sensor chip is sensitive enough in a wide concentration range. The result shows our sensor chip is practical and accurate for high-throughput CRP detecting in clinical diagnostics.

4. Conclusion

A label-free, high-throughput and low-cost biosensor for the binding kinetics quantification of CRP in human blood serum based on nanoplasmonic sensor in microplate wells by generic plate reader is presented. The sensitivity of the sensor is 566 Δ%T/RIU at λ = 565 nm while 450 Δ%T/RIU at λ = 705 nm. We achieved detection of inflammation biomarker CRP with a LOD of 50 ng/ml which has full capacity of detecting CRP in blood serum with high consistency with from hospital test. Furthermore, the nanoplasmonic sensor microplate is also a powerful tool for studying dynamic protein interaction and measuring binding kinetics. We can realize similar functionality of commercial SPR systems by simply utilizing the ubiquitous microplate reader. The unique nanosensor plate combined with generic microplate reader may become a new technology platform for biomolecular interaction and kinetic study.

CRediT authorship contribution statement

Tang Dang: Conceptualization, Methodology, Investigation, Data curation, Visualization, Writing - original draft. **Wenjun Hu:** Funding acquisition, Conceptualization, Investigation, Writing - review & editing, Resources. **Wei Zhang:** Software. **Zifang Song:** Resources. **Yi Wang:** Software. **Mingqian Chen:** Data curation. **Hao Xu:** Supervision, Funding acquisition. **Gang Logan Liu:** Supervision, Writing - review & editing, Funding acquisition, Project administration.

Acknowledgment

This work was supported by Huazhong University of Science and Technology and National Natural Science Foundation of China (grant 81602111), General Financial Grant from the China Postdoctoral Science Foundation (grant 2016M592675).

Appendix A. Supplementary data

Supplementary data to this article can be found online at https://doi.org/10.1016/j.bios.2019.111494.

Declaration of interests

The authors declare that they have no known competing financial interests or personal relationships that could have appeared to influence the work reported in this paper.

References

Ala-Kleme, T., Mäkinen, P., Ylinen, T., Väre, L., Kulmala, S., Ihalainen, P., Peltonen, J., 2006. Anal. Chem. 78 (1), 82–88.
Arlett, J., Myers, E., Roukes, M., 2011. Nat. Nanotechnol. 6 (4), 203.
Boccaletti, S., Latora, V., Moreno, Y., Chavez, M., Hwang, D.-U., 2006. Phys. Rep. 424 (4–5), 175–308.
Bohren, C., Huffman, D., 1983. Absorption and Scattering of Light by Small Particles. Wiley New York Google Scholar.
Bryan, T., Luo, X., Bueno, P.R., Davis, J.J., 2013. Biosens. Bioelectron. 39 (1), 94–98.
Cheng, M.M.-C., Cuda, G., Bunimovich, Y.L., Gaspari, M., Heath, J.R., Hill, H.D., Mirkin, C.A., Nijdam, A.J., Terracciano, R., Thundat, T., 2006. Curr. Opin. Chem. Biol. 10 (1), 11–19.
Choi, Y.-H., Ko, H., Lee, G.-Y., Chang, S.-Y., Chang, Y.W., Kang, M.-J., Pyun, J.-C., 2015. Sensor. Actuator. B Chem. 207, 133–138.
Chou, C., Hsu, H.-Y., Wu, H.-T., Tseng, K.-Y., Chiou, A.E., Yu, C.-J., Lee, Z.-Y., Chan, T.-S., 2007. J. Biomed. Opt. 12 (2), 024025.
Christodoulides, N., Mohanty, S., Miller, C.S., Langub, M.C., Floriano, P.N., Dharshan, P., Ali, M.F., Bernard, B., Romanovicz, D., Anslyn, E., 2005. Lab Chip 5 (3), 261–269.
Crystal, R.G., Bitterman, P.B., Rennard, S.I., Hance, A.J., Keogh, B.A., 1984. N. Engl. J. Med. 310 (3), 154–166.
D'Orazio, P., 2003. Clin. Chim. Acta 334 (1–2), 41–69.
Ding, P., Liu, R., Liu, S., Mao, X., Hu, R., Li, G., 2013. Sensor. Actuator. B Chem. 188, 1277–1283.
Fabini, E., Fiori, G.M.L., Tedesco, D., Lopes, N.P., Bertucci, C., 2016. J. Pharm. Biomed. Anal. 122, 166–172.
Homola, J., 2008. Chem. Rev. 108 (2), 462–493.
Hotamisligil, G.S., 2006. Nature 444 (7121), 860.
Jason-Moller, L., Murphy, M., Bruno, J., 2006. Current protocols in protein science 45 (1) 19.13. 11-19.13. 14.
Justino, C.I., Freitas, A.C., Amaral, J.P., Rocha-Santos, T.A., Cardoso, S., Duarte, A.C., 2013. Talanta 108, 165–170.
Koivunen, M.E., Krogsrud, R.L., 2006. Lab. Med. 37 (8), 490–497.
Lee, G.-Y., Park, M., Kang, M.-J., Langer, K., Jose, J., Pyun, J.-C., 2018. Sensor. Actuator. B Chem. 258, 1131–1137.
Leonard, P., Hearty, S., O'Kennedy, R., 2011. Protein Chromatography. Springer, pp. 403–418.
Maynard, J.A., Lindquist, N.C., Sutherland, J.N., Lesuffleur, A., Warrington, A.E., Rodriguez, M., Oh, S.-H., 2009. Biotechnol. J. 4 (11), 1542.

Meyer, M.H.F., Hartmann, M., Keusgen, M., 2006. Biosens. Bioelectron. 21, 1987–1990.
Nguyen, H., Park, J., Kang, S., Kim, M., 2015. Sensors 15 (5), 10481–10510.
O'Shannessy, D., Brigham-Burke, M., Soneson, K., Hensley, P., Brooks, I., 1993. Anal. Biochem. 212 (2), 457.
Olaru, A., Bala, C., Jaffrezic-Renault, N., Aboul-Enein, H.Y., 2015. Crit. Rev. Anal. Chem. 45 (2), 97–105.
Pepys, M.B., Hirschfield, G.M., 2003. J. Clin. Investig. 111 (12), 1805–1812.
Phurimsak, C., Tarn, M.D., Peyman, S.A., Greenman, J., Pamme, N., 2014. Anal. Chem. 86 (21), 10552–10559.
Reeves, G., 2007. Aust. Prescr. 30 (3), 74–76.
Ridker, P.M., Buring, J.E., Shih, J., Matias, M., Hennekens, C.H., 1998. Circulation 98 (8), 731–733.
Songjaroen, T., Feeny, R.M., Mensack, M.M., Laiwattanapaisal, W., Henry, C.S., 2016. Sensing and bio-sensing research 8, 14–19.
Vance, S.A., Sandros, M.G., 2014. Sci. Rep. 4, 5129.
Wang, W., Mai, Z., Chen, Y., Wang, J., Li, L., Su, Q., Li, X., Hong, X., 2017. Scientific reports 7 (1), 16904.
Wijaya, E., Lenaerts, C., Maricot, S., Hastanin, J., Habraken, S., Vilcot, J.-P., Boukherroub, R., Szunerits, S., 2011. Curr. Opin. Solid State Mater. Sci. 15 (5), 208–224.
Williams Jr., D.K., Muddiman, D.C., 2009. J. Proteome Res. 8 (2), 1085–1090.
Yeom, S.-H., Han, M.-E., Kang, B.-H., Kim, K.-J., Yuan, H., Eum, N.-S., Kang, S.-W., 2013. Sensor. Actuator. B Chem. 177, 376–383.